ЖУРНАЛ СТРУКТУРНОЙ ХИМИИ

2012. Том 53, № 4 *Июль – август* *С. 678 – 686*

UDC 541.6:541.49:546.72

DFT CHARACTERIZATION OF 1-ACETYLPIPERAZINYLDITHIOCARBAMATE LIGAND AND ITS TRANSITION METAL COMPLEXES

S.A. Beyramabadi, A. Morsali, S.H. Vahidi

Department of Chemistry, Mashhad Branch, Islamic Azad University, Mashhad, Iran,
e-mail: beiramabadi6285@mshdiau.ac.ir

Received January, 24, 2011

Employing DFT and handling the solvent effects with the PCM model, the 1-acetylpiperazinyldithiocarbamate acpdtc ligand and its $M(acpdtc)_2$ complexes, where M is Mn(II), Fe(II), Co(II), Ni(II) and Cu(II), are characterized computationally. The obtained results suggest that the piperazine ring adopts *chair* conformation in all the studied species. In the gas and solution phases, the *chair* form of the ligand is dominant. For the Mn, Fe and Co complexes the tetrahedral structure is more stable than the square form in the gas and solution phases. However, the Ni and Cu complexes adopt the square form, in which the complex has the inversion center. The calculated vibrational frequencies are in agreement with the experimental ones, confirming the suitability of the optimized geometries of the compounds. Atomic charges, electron distribution of the frontier orbitals, and stabilizing electron transfers are determined by the NBO analysis.

K e y w o r d s: density functional theory; PCM; Schiff base; IR assignment; NBO; dithiocarbamate; piperazine.

INTRODUCTION

Due to their versatile binding ability, dithiocarbamato ligands form complexes with most transition metals [1—6]. In addition, dithiocarbamates have received increasing attention in recent years because of their various biological activities, such as anticancer [1, 2], antiviral [7], NO-trapping agent [8], myocardial tracer [9], AIDS therapy [10], and especially the production of a wide spectrum of fungicides [6, 11]. Moreover, they are suitable for diverse industrial usage, including the manufacture of pesticides [12], apart from their uses in materials science [4] as well as the use of dithiocarbamate linkers for the improvement of electron transport properties in molecular wire junctions [13].

On the other hand, piperazine and its derivatives represent an interesting class of heterocyclic diamine ligands. From a biological point of view, they can be used for a wide range of applications as kinase inhibitor [14], drug agent [15], myocardial imaging agent [9], anticancer agents [16], antimuscarinic and antibacterial activities [17, 18], pharmacological application due to the psychotropic activity [19], treatment of cocaine abuse [20], and so on [6]. Many metal complexes of piperazine and its derivatives have been synthesized [4, 6, 21], and some of them display interesting biological activities such as the DNA cleavage [21] and antifungal activities [6].

Regarding all the points mentioned above, it is expected that compounds containing both dithiocarbamate and piperazine groups will have many useful and applied peculiarities that will consequently make their study very attractive. Among the compounds synthesized from this group is 1-acetylpiperazinyldithiocarbamate, which has recently been synthesized by Mohammad et al. [6], and no theoretical studies have yet been reported for this compound.

Now, theoretical investigations have much applicability in the investigation of chemical reactions [22—25] and the identification of chemical compounds [21, 26—30]. They could, at the same time, be considered as complementary to or replacement for experimental methods. Previously, these calculations have been used for the investigation of dithiocarbamates as well as the piperazine compounds [3, 21, 27—29].

The aim of this work is a comprehensive DFT characterization of the titled ligand and its metal complexes, including the optimization of plausible geometries, determination of structural parameters, determination of the most stable structure for each species, assignment of the IR spectra, and the natural bond orbital (NBO) analysis. For more clarification, we have used here the abbreviation acpdtc for this ligand, as used in the experimental paper [6].

THEORETICAL METHODS

All calculations have been performed with the Gaussian 03 software package [31] using gradient-corrected DFT with the B3LYP functional [32]. The 6-31G(*d*,*p*) basis set was employed, except for the metal atoms, in which the LANL2DZ basis set was used with including effective core potential functions.

All degrees of freedom were optimized for all the geometries. The optimized geometries were confirmed to have no imaginary frequency of the Hessian. In the gas phase, the frequency calculations were performed to evaluate the zero-point and the Gibbs free energies.

In this work, one of the self-consistent reaction field methods (the sophisticated Polarizable Continuum Model (PCM) [33]) has been employed for the investigation of solvent effects. The gas-phase optimized geometries were used to treat the solvent effects. Also, calculations of the atomic charges and NBO analysis were performed on the optimized geometries.

The DFT calculated wavenumbers are usually higher than the experimental values [27, 30, 34]. Here, the scale factor of 0.9614 was used for the correction of the calculated wavenumbers [34].

RESULTS AND DISCUSSION

Mohammad et al. [6] have recently synthesized the acpdtc ligand and its $M(acpdtc)_2$-type metal complexes, where M involves Mn(II), Fe(II), Co(II), Ni(II), and Cu(II) transition metals. Since no crystal structural data have been reported for the acpdtc ligand and its complexes, the determination of their structural parameters is valuable.

Here, their geometries were fully optimized and the obtained results were compared with the reported data for the similar compounds [1, 3, 27, 35—42]. Also, the stability of possible structures of the compound has been computationally studied in the gas phase as well as in the methanol solution. Then, the NBO analysis and frequency assignments have been performed on the gas-phase optimized geometries.

acpdtc Ligand. The acpdtc ligand can exist as both *chair* and *boat* conformations, and their geometries have been fully optimized in the gas phase. Their selected structural parameters are gathered in Table 1, together with the experimental values of the similar compounds. As seen, the calculated structural parameters are in good agreement with the experimental ones [1, 3, 27, 35—42].

The optimized geometries of the *chair* and *boat* conformations of acpdtc are shown in Fig. 1. In both conformations, dithiocarboxylate and acetyl groups are in the same plane with N1 and N2 atoms respectively. There are some structural differences between the *chair* and *boat* conformations, the most important of which have been presented below.

Contrary to the *boat* form, four carbon atoms of the piperazine ring are essentially in the same plane for the *chair* conformation. For the *chair* conformation, the calculated C1—C2—C3—C4 and C1—N1—N2—C6 dihedral angles are –0.6° and –21.6° respectively, which are 51.5° and 179.8° for the *boat* one respectively. Also, the calculated C1—N1—N2 and N1—N2—C6 angles obviously show distinct differences between the *chair* and *boat* conformations of the acpdtc ligand.

According to our calculations, the *boat* conformation is less stable than the *chair* conformation by 4.05 kcal/mol in the gas phase. Treatment of solvent effects reduces this energy difference to 3.85 kcal/mol.

Table 1

Optimized structural parameters of the acpdtc *ligand and its complexes*

	Experimental	Calculated						
		Ligand (*Chair*)	Ligand (*Boat*)	Mn complex	Fe complex	Co complex	Ni complex	Cu complex
		Bond length, pm						
C1—S1	170.0 [3], 172.1 [41], 171.6 [42], 172.7 [44], 172.8 [45], 172.8 [46], 171.4 [47], 172.0 [48]	172.0	1.721	174.5	174.6	174.1	173.0	173.4
C1—S2	169.0 [3], 172.7 [42], 174.1 [43]	172.2	1.723	174.6	174.7	174.2	173.1	173.5
C1—N1	134.4 [41], 132.5 [42], 132.4 [43], 132.3 [44], 132.4 [47], 131.6 [48]	140.1	1.395	134.5	134.3	134.2	134.1	134.3
N1—C2	146.2 [31], 147.3 [42], 145.7 [45]	145.6	1.460	147.4	147.4	147.4	147.1	147.2
C2—C3	153.8 [31], 151.9 [42]	153.5	1.526	153.3	153.3	153.4	153.3	153.3
C3—N2	146.4 [31]	146.6	1.470					
C6—N2	136.0 [31]	135.5	1.352	136.9	136.9	136.9	136.9	136.9
C6—O	122.8 [31]	122.7	1.227	121.9	121.8	121.8	121.8	121.8
M—S	241.0 [3], 220.9, 227.6 [41], 231.9 [42], 230.8 [43], 231.5 [44], 221.5 [45], 220.9 [46], 220.3 [47], 220.7 [48]	—	—	249.4	241.7	239.8	228.0	239.8
		Angle, deg.						
S1—C1—S2	121.6 [3], 111.6 [42], 112.4 [43], 112.5 [44], 108.3 [45], 110.6 [46], 110.2 [47], 109.9 [48]	123.7	124.5	118.8	117.6	116.2	112.6	115.4
S1—C1—N1	123.6, 121.8 [41], 124.4 [42], 123.3 [43], 122.9 [44], 124.6 [45], 124.5 [46], 124.7 [47], 124.8 [48]	118.2	117.2	120.6	121.3	121.9	123.7	122.3
N1—C2—C3	109.2 [42]	110.6	111.6	110.1	110.0	110.0	110.1	110.1
C2—C3—N2	113.9 [31]	110.6	110.5	110.4	110.4	110.4	110.3	110.3
N2—C6—O	122.8 [31]	126.6	125.6	125.2	125.1	125.1	125.1	125.1
C1—M—C1′	0.0 [42], 4.4 [44], 1.9 [46], 0.0 [48]	—	—	178.9	179.4	179.3	180.0	180.0
S1—M—S2	75.6 [3], 75.5 [42], 76.2 [43], 77.0 [44], 78.6 [45], 79.4 [46], 79.4 [47], 79.4 [48]	—	—	74.1	76.3	76.1	78.3	75.3
S1—M—S1′	180.0 [42], 176.8 [46], 180.0 [47], 180.0 [48]	—	—	129.8	127.3	128.3	180.0	180.0
S1—M—S2′	104.5 [42], 104.9 [44], 100.3 [46], 100.6 [47], 100.6 [48]	—	—	130.5	129.0	129.0	101.7	104.6
		Dihedral Angle, deg.						
S1—C1—N1—C4	172.3 [42], –1.5 [43]	175.3	–2.6	179.3	179.1	179.5	179.6	179.6
C1—N1—C4—C5	107.7 [42]	111.0	163.1	119.4	119.7	120.2	122.3	121.8
C4—C5—N2—C6	–128.0 [31]	125.5	139.3	123.9	123.8	123.7	122.7	123.3
C5—N2—C6—O	–174.4 [31]	–178.2	179.9	–177.9	–178.0	–177.9	–177.6	–177.7
S1—S2—S2′—S1′	0.0 [42], 0.1 [46], 0.0 [47], 0.0 [48]	—	—	81.6	80.1	81.3	0.0	0.0
M—S1—C1—S2	5.8 [42], 5.2 [43], 5.2 [44], –3.5 [45], 3.6 [46], 2.3 [47], 3.0 [48]	—	—	0.0	0.1	0.0	0.2	0.0
N1—C2—C2′—N1′	180.0 [42], 179.0 [46], 180.0, 179.0 [47]	—	—	11.6	23.2	0.8	179.6	176.2

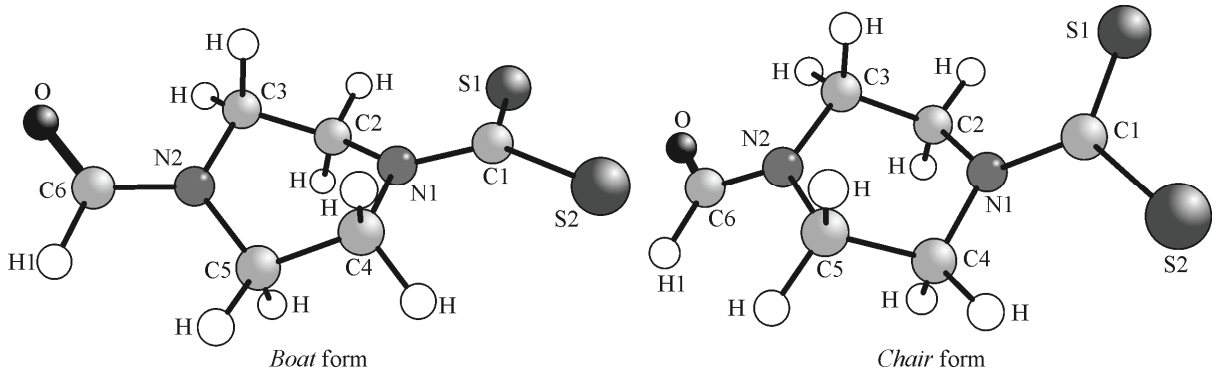

Fig. 1. Optimized structures of the *boat* and *chair* conformers of the acpdtc ligand

With regard to the equilibrium between the *chair* and *boat* conformers, the conformation equilibrium constant (K) could be calculated by

$$K = \exp\left(-\frac{\Delta G}{RT}\right) \quad (1)$$

where ΔG, R, and T are the Gibbs free energy difference between the two conformers, the gas constant, and temperature respectively. In both the gas and solution phases, ΔGs are in favor of the *chair* form by 2.40 kcal/mol and 2.08 kcal/mol respectively. Hence, using eq. 1, the amount of the *boat* form is predicted to be negligible (1.71 % and 2.90 % in the gas phase and the methanol solution respectively).

M(acpdtc)$_2$ complexes. In the optimized geometries of the complexes, the anionic acpdtc ligand acts as a symmetrical bidentate ligand chelating to metal ions through the sulfur atoms, where the piperazine rings have the *chair* conformation. For the acpdtc ligand as well as all the complexes, two C—S bond lengths are essentially the same, confirming the delocalization of the electron density between the C—S bonds.

Here, two possible structures were investigated for each complex, tetrahedral and square planar. The obtained results are discussed below.

Mn, Fe, and Co complexes. Each of the Mn, Fe and Co complexes could exist as tetrahedral or square structures. The square structure as an input file is converted to the tetrahedral structure in the output file. Only for the Co complex, we succeed to optimize the square structure. Important structural parameters of the tetrahedral form of these complexes are gathered in Table 1, which are in good agreement with the experimental values [1, 3, 27, 35—42].

The optimized structures of the tetrahedral and square forms are shown in Fig. 2. The acpdtc ligands coordinate via the sulfur atoms forming two four-membered chelating rings around the metal ions, which make approximately an 80° dihedral angle to each other. The calculated S1—S2—S2′—S1′ dihedral angles of the Mn, Fe and Co complexes are 81.6°, 80.1°, and 81.3° respectively. The elongation of the C—S bond from 1.72 Å for the free ligand to about 1.74 Å for the M(acpdtc)$_2$ complexes and a decrease in the S1—C1—S2 angle are arisen from the reduction of the electron density on the coordinated sulfur atoms.

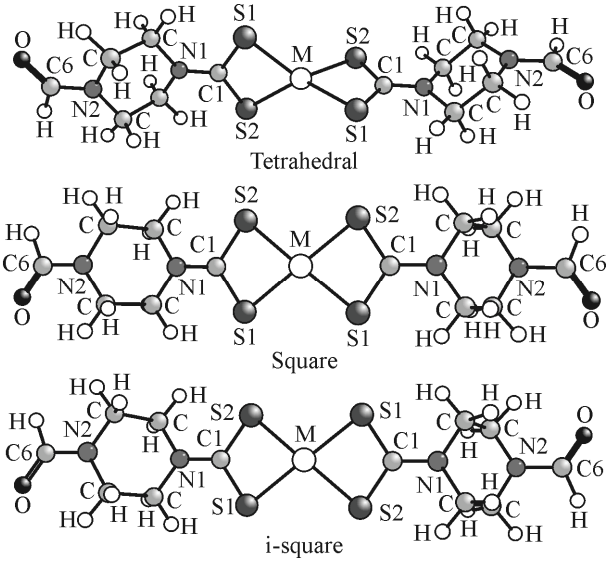

Fig. 2. Optimized structures of the three possible structures of M(acpdtc)$_2$ complexes

For the Co complex, the calculations implied that the tetrahedral form is more stable than the square one in the gas and solution phases. In the gas phase, the energy difference between the tetrahedral and square forms is 4.71 kcal/mol, which increases to 6.20 kcal/mol by considering the solvent effects. Moreover, ΔG of this complex is in favor of the tetrahedral form: 5.19 kcal/mol and 5.86 kcal/mol in the gas and solution phases respectively. Hence, using eq. 1, the amount of the square form for the Co complex is predicted to be dispensable (0.0051 %) in the methanol solution.

Ni and Cu complexes. Each of the Ni and Cu complexes can exist as tetrahedral or square structures, the geometries of which were fully optimized. The optimized structures for Ni and Cu complexes are similar to each other and to some extent similar to the optimized structures for the complexes of the previous group (Fig. 2). The tetrahedral and square structures of the two complexes include many differences, the most important of which have been mentioned below.

In the square planar form, the coordinating sulfur atoms are in the same plane, whereas in the tetrahedral form, the two four-membered chelating rings are roughly perpendicular to each other. The calculated S1—S2—S2′—S1′ dihedral angles for the square and tetrahedral forms are about 0.0° and 82.1° respectively. In the square form, the M—S bond lengths are shorter by about 0.1 Å.

In the square form of the complexes, depending on the orientation of two —CHO groups relative to each other, two different structures are possible. In the more symmetric structure, C—H and C=O bonds of each —CHO group with their corresponding bonds in another —CHO group are situated on two opposite sides of the complex and are symmetric to each other, so that the Ni and Cu complexes have an inversion center. But in another form, the corresponding bonds in both —CHO groups are on the same side of the complexes and the complexes have no center of symmetry (Fig. 2). From now on, we call these two different forms of the square structure as *i*-square and square forms respectively.

The obtained structures for *i*-square and square forms of the complexes have slight differences. The important structural parameters of the *i*-square form are gathered in Table 1, which are in good agreement with the experimental data reported for the similar compounds [1, 3, 27, 35—42].

Based on the computed relative energies, the *i*-square form is more stable than the square form in both complexes. For the Ni complex, energy differences between the two square forms are 3.61 kcal/mol and 0.09 kcal/mol in the gas and solution phases respectively, which are 0.1 kcal/mol and 2.33 kcal/mol respectively for the Cu complex. Moreover, ΔGs were found to be in favor of the *i*-square form. In the methanolic solution, ΔG between the two square forms of the Ni complex is 0.54 kcal/mol, resulting to 71.33 % for the *i*-square form in the solution. For the Cu complex, ΔG is 2.30 kcal/mol, predicting 97.9 % for the *i*-square form in the methanol solution. Hence, using eq. 1, the *i*-square is dominant form in the square $\rightleftharpoons$ *i*-square equilibrium.

For the Ni and Cu complexes, the tetrahedral structure is less stable than the *i*-square one by about 10 kcal/mol in the methanol solution. Also, the Gibbs free energies favor the square form in comparison with the tetrahedral form, so that the Ni and Cu complexes include only the square form in the gas and solution phases.

Regarding the relative energies calculated, it is concluded that the tetrahedral form is the most stable for the Mn, Fe and Co complexes and the *i*-square is the most stable form for the Ni and Cu complexes. Subsequently, the results obtained from the vibrational IR assignment and NBO analysis have been presented, which have been calculated on the most stable structure of each species.

Vibrational spectroscopy. Theoretical assignment of the spectra is playing a significant role in the identification of chemical compounds [27, 30]. Here, theoretical assignments of the IR bands were performed on the most stable geometries of the $(acpdtc)^-$ ligand, K(acpdtc) and $M(acpdtc)_2$ complexes. The optimized geometry of K(acpdtc) is shown in Fig. 3, in which the piperazine ring has the *chair* conformation.

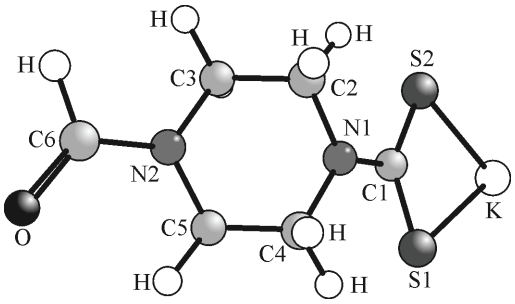

Fig. 3. Optimized structure of K(acpdtc)

Table 2

Selected experimental and theoretical IR vibrational frequencies (cm^{-1}) *of* K (acpdtc), *the tetrahedral form of the* Mn, Fe, *and* Co *complexes, and the i-square form of the* Ni *and* Cu *complexes*

Theor.						Exp.						Assignment
K(acpdtc)	Mn	Fe	Co	Ni	Cu	K(acpdtc)	Mn	Fe	Co	Ni	Cu	
	346	348	343	361	334							υ_{sym}(M—S)
	391	408	391	378	379							υ_{asym}(M—S)+ $+\delta_{scissoring}$(S—C—S)
507	504	503	506	510	508		500	478	524	519	516	$\delta_{out\ of\ planep}$(Cof CS2, N bonded to CHO)+ $+\upsilon_{asym}$(M—S)
785	785	783	785	785	785		759	763	760	760	762	breathing of the piperazine ring
962	972	971	972	979	975		991	1004	987	984	987	υ_{asym}(S—C—S)+ $+\upsilon_{asym}$(C—N, C—C) piperazine ring
987	986	986	986	987	986							υ_{sym}(C—N, C—C) piperazine ring
1378	1378	1378	1378	1377	1377							$\delta_{in\ plane}$(H aldehyde)
1410	1408	1407	1407	1407	1407	1454	1480	1482	1484	1481	1484	υ(C—N)acetyl
1385	1461	1463	1465	1467	1463							υ(C—N)dithiocarbamate
1726	1731	1731	1731	1731	1731	1631	1630	1638	1637	1646	1635	υ(C=O)
2833	2846	2846	2846	2846	2846							υ(C—H aldehyde)
2905–2926	2912–2941	2912–2942	2912–2941	2914–2938	2913–2938							$\upsilon_{sym}(CH_2)$ piperazine ring
2980	2988	2989	2989	2989	2989							$\upsilon_{asym}(CH_2)$ piperazine ring

The important results of the IR assignments are listed in Table 2, together with the corresponding experimental values for comparison. As seen, the theoretical results are in good agreement with the experimental values, confirming the suitability of the optimized geometries for the studied species.

Weak bands in the 330—510 cm^{-1} region of the IR spectra of $M(acpdtc)_2$ complexes can be assignned to the M—S stretching vibrations associated with other vibrations (Table 2). At 500—510 cm^{-1}, the M—S stretching vibration is weaker than the bending modes.

The υ(C—S) band is of particular interest since its energy is diagnostic of the coordination mode of dithiocarbamate ligands [6]. The DFT calculations suggest that the asymmetric S—C—S stretching vibration of the anionic acpdtc ligand results in a weak to medium band at 987 cm^{-1}, which is associated with the asymmetric stretching vibrations of the piperazine rings. By complexation, this band shifts considerably to lower energies (972—979 cm^{-1}) in the spectra of the complexes.

One of the interesting obtained results is the assignment of the υ(C—N) vibration. The C—N stretching vibrations of the acetyl and NCSS moieties result in two strong bands at about 1410 cm^{-1} and 1385 cm^{-1} in the IR spectrum of the K(acpdtc), while the later one involves higher intensity. Compared to the IR spectrum of K(acpdtc), the former vibration appears in the same region in the IR spectra of the complexes, whereas υ(C—N) of NCSS moiety shifts considerably to higher energies (by about 80 cm^{-1}), indicating the electron delocalization toward the metals. The overlap of these C—N stretching vibrations leads to a band broading in the experimental IR spectra [6]. A strong band at about 986 cm^{-1} of the IR spectra arises from the symmetric stretching modes of the C—C and C—N bonds of the piperazine rings.

For all the species, the highest intensity band appears at about 1730 cm^{-1}, which was assigned to the stretching vibration of the C=O bond. Only for this vibration, the experimental and calculated

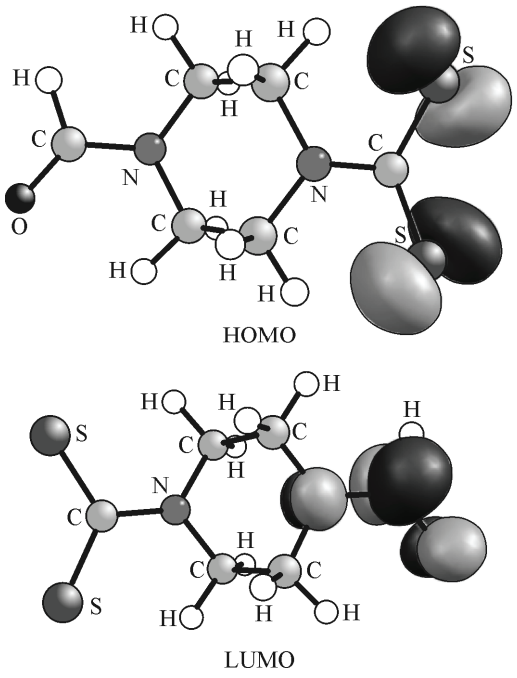

Fig. 4. 3D maps of the HOMO and LUMO frontier orbitals of the *chair* conformer of acpdtc

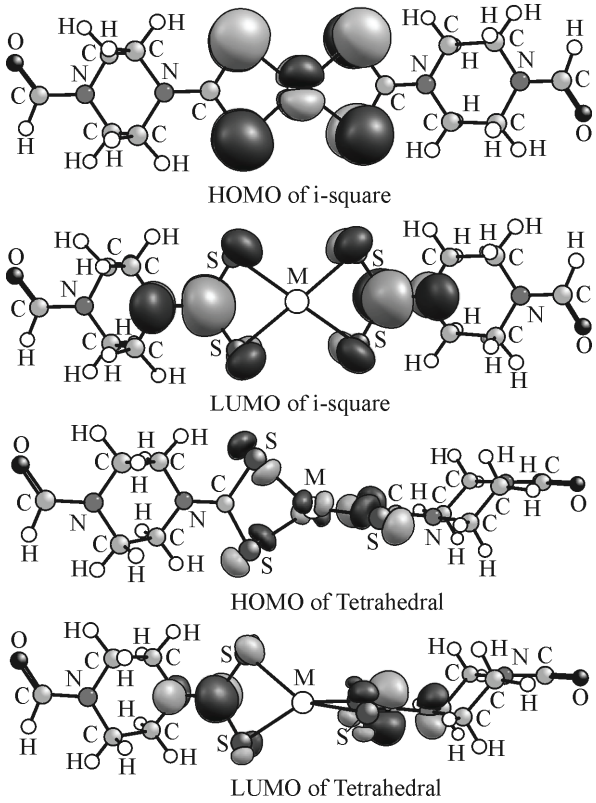

Fig. 5. 3D maps of the HOMO and LUMO frontier orbitals of $M(acpdtc)_2$ complexes

wavenumbers show a substantial difference that can be attributed to the intermolecular interactions in the solid state, which are not considered in the gas phase calculations for the isolated molecule.

The C—H stretching modes result in the appearance of some bands in the 2900 cm^{-1} to 3000 cm^{-1} region of the IR spectra, in which aldehyde υ(C—H) has the highest intensity.

NBO analysis. The NBO analysis is a valuable approach for the investigation of molecular bonding interactions, atomic charges, and charge transfer in chemical compounds [43, 44]. The important results of the NBO analysis of the ligand and its complexes are listed below.

The distributions of the frontier orbitals for the acpdtc ligand have been shown in Fig. 4. As seen, the highest occupied molecular orbital (HOMO) is localized on the *p* orbitals of the S atoms, whereas the lowest unoccupied molecular orbital (HOMO) is localized on the *p* orbitals of the N, C, and O atoms. Their energy difference is 4.00 kcal/mol, indicating the stability of this species.

Going from Mn to Cu complexes, the positive charge on the first-row-transition metal decreases along with the electron density on the bonded S atoms. The 3D map of the HOMOs and LUMOs of $M(acpdtc)_2$ complexes is shown in Fig. 5. For the *i*-square complexes (Ni and Cu), the electron cloud of HOMOs is mainly localized on the coordinated S atoms, whereas LUMOs are mainly localized on the C and N atoms, with low density on the S atoms. For the three tetrahedral complexes (Mn, Fe, and Co), HOMO shows the electron delocalization on the *d* orbital of the metal atom and the *p* orbitals of the S atoms. The LUMO electron cloud is localized on the NCSS fragment, where the order of the electron density on the atoms is C > N > S1, S2 (Fig. 5). The HOMO-LUMO energy gaps for the Mn to Cu complexes are in the range of 4.20—4.83 eV, which are large in magnitude.

The stabilization energy ($E(2)$) resulting from electron delocalization between donor NBO(i) and acceptor NBO(j) orbitals is evaluated as

$$E(2) = -q_i \frac{(F_{ij})^2}{\varepsilon_j - \varepsilon_i} \tag{2}$$

Table 3

B3LYP/6-31G(*d*,*p*) *calculated energy of hyper conjugative interactions* (kcal/mol) *for the* acpdtc *ligand and its complexes by* NBO *analysis*

Donor NBO (*i*)	Acceptor NBO (*j*)	acpdtc	Complexes				
			Mn	Fe	Co	Ni	Cu
LP(1) N1	LP*(1) C6		64.07	64.03	64.00		63.66
LP(1) N1	BD*(1) C6—O1	37.66	—	—	—	—	—
LP(1) N2	LP*(1) C5	55.94	91.02	92.49	91.29		91.98
LP(3) S1	LP*(1) C5	114.81	72.43	69.98	72.20		72.61
LP(3) S2	LP*(1) C5	119.22	73.45	71.04	73.41		73.58
LP(1) O1	LP*(1) C6		159.73	160.74	160.60		160.74
LP(1) O1	BD*(1) N1—C6		12.50	12.51	12.51		12.52
LP(2) S1	LP*(6) M		24.22	29.82	29.57		26.88
LP(2) S2	LP*(6) M		24.61	30.24	29.84		27.13

where q_i, F_{ij}, ε_j, and ε_i parameters are the donor orbital occupancy, the off-diagonal NBO Fock matrix element, and the energies of the acceptor and donor orbitals respectively. The variables of Eq. 2 were obtained from the second-order perturbation theory analysis of the Fock matrix in the NBO basis. The greater electron transfer from the electron donor to the acceptor leads to higher stabilization energy.

Some electron transfers are gathered in Table 3, which show high stabilizing energy. For the acpdtc ligand, the strongest electron donations belong to $n(\mathrm{S}) \rightarrow n^*$ (C5) NBO interactions. In the $M(acpdtc)_2$ complexes, these interactions are weaker because of a lower negative charge on the S atoms. Inversely, by creating the electron density deficiency on C5, $n(\mathrm{N2}) \rightarrow n^*$ (C5) electron transfer increases. The electron transfer interactions result in the electron delocalization in the NCSS fragment.

For the complexes, $n(\mathrm{O1}) \rightarrow n^*$ (C6) electron transfer is the strongest one and $n(\mathrm{S}) \rightarrow n^*$ (M) charge transfer considerably stabilizes the complexes.

CONCLUSIONS

In this work, the plausible structures of the acpdtc ligand and its $M(acpdtc)_2$ complexes have been characterized using the DFT methods. The most stable structure of each species was determined, in which piperazine has the *chair* conformation for all the studied species.

The acpdtc ligand adopts the *chair* conformation in both gas and solution phases. The Mn, Fe, and Co complexes have the tetrahedral structure in the gas phase and the methanol solution. As for the Ni and Cu complexes, the most stable geometry was found to be a symmetric square structure, in which the complex has an inversion center. The calculated IR frequencies are good in agreement with the experimental frequencies, confirming the suitability of the optimized geometries for the investigated species. Also, the NBO analysis shows that the strongest electron donations of the acpdtc ligand and $M(acpdtc)_2$ complexes are $n(\mathrm{S}) \rightarrow n^*$ (C5) and $n(\mathrm{O1}) \rightarrow n^*$ (C6) donations respectively.

REFERENCES

1. *Ronconi L., Marzano C., Zanello P., Corsini M., Miolo G., Maccà C., Trevisan A., Fregona D.* // J. Med. Chem. – 2006. – **49**, N 5. – P. 1648 – 1657.
2. *Ronconi L., Giovagnini L., Marzano C., Bettìo F., Graziani R., Pilloni G., Fregona D.* // Inorg. Chem. – 2005. – **44**, N 6. – P. 1867 – 1881.
3. *Mire L.W., Marynick D.S.* // Inorg. Chem. – 2000. – **39**, N 26. – P. 5970 – 5975.
4. *Wilton-Ely J.D.E.T., Solanki D., Knight E.R., Holt K.B., Thompson A.L., Hogarth G.* // Inorg. Chem. – 2008. – **47**, N 20. – P. 9642 – 9653.
5. *Mazalov L.N., Bausk N.V., Érenburg S.B., Larionov S.V.* // J. Struct. Chem. – 2001. – **42**, N 5. – P. 784 – 793.
6. *Mohammad A., Varshney C., Nami S.A.A.* // Spectrochim. Acta Part A. – 2009. – **73**, N 1. – P. 20 – 24.
7. *Sohn R.H., Deming C.B., Johns D.C., Champion H.C., Bian C., Gardner K., Rade J.J.* // Blood. – 2005. – **105**, N 10. – P. 3910 – 3917.

8. *Lu D., Nadas J., Zhang G., Johnson W., Zweier J.L., Cardounel A.J., Villamena F.A., Wang P.G.* // J. Amer. Chem. Soc. – 2007. – **129**, N 17. – P. 5503 – 5514.
9. *Bolzati C., Cavazza-Ceccato M., Agostini S., Refosco F., Yamamichi Y., Tokunaga S., Carta D., Salvarese N., Bernardini D., Bandoli G.* // Bioconjugate Chem. – 2010. – **21**, N 5. – P. 928 – 939.
10. *Lang J.M., Touraine J.L., Trepo C., Choutet P., Kirstetter M., Falkenrodt A., Herviou L., Livrozet J.M., Retornaz G., Touraine F.* // Lancet. – 1988. – **2**, N 8613. – P. 702 – 706.
11. *Pedras M.S.C.* // Chem. Rec. – 2008. – **8**, N 2. – P. 109 – 115.
12. *Viquez O.M., Valentine H.L., Friedman D.B., Olson S.J., Valentine W.M.* // Chem. Res. Toxicol. – 2007. – **20**, N 3. – P. 370 – 379.
13. *Li Z., Kosov D.S.* // J. Phys. Chem. B. – 2006. – **110**, N 20. – P. 9893 – 9898.
14. *Das J., Chen P., Norris D., Padmanabha R., Lin J., Moquin R.V., Shen Z., Cook L.S., Doweyko A.M., Pitt S., Pang S., Shen D.R., Fang Q., de Fex H.F., McIntyre K.W., Shuster D.J., Gillooly K.M., Behnia K., Schieven G.L., Wityak J., Barrish J.C.* // J. Med. Chem. – 2006. – **49**, N 23. – P. 6819 – 6832.
15. *Ferreira S.H., Lorenzetti B.B., Devissaguet M., Lesiuer D., Tsouderos Y.* // Br. J. Pharmacol. – 1995. – **114**, N 2. – P. 303 – 308.
16. *Jain A.K., Reddy V.V., Paul A., Muniyappa K., Bhattacharya S.* // Biochemistry. – 2009. – **48**, N 45. – P. 10693 – 10704.
17. *Kaiser C., Audia V.H., Carter J.P., McPherson D.W., Waid P.P., Lowe V.C., Noronha-Blob L.* // J. Med. Chem. – 1993. – **36**, N 5. – P. 610 – 616.
18. *Ziegler C.B., Bitha P., Kuck N.A., Fenton T.J., Petersen P.J., Lin Y.* // J. Med. Chem. – 1990. – **33**, N 1. – P. 142 – 146.
19. *Schut R.N., Ward F.E., Rodriguez R.* // J. Med. Chem. – 1972. – **15**, N 3. – P. 301 – 304.
20. *Cao J., Kulkarni S.S., Husbands S.M., Bowen W.D., Williams W., Kopajtic T., Katz J.L., George C., Newman A.H.* // J. Med. Chem. – 2003. – **46**, N 13. – P. 2589 – 2598.
21. *Chattopadhyay T., Mukherjee M., Mondal A., Maiti P., Banerjee A., Banu K.S., Bhattacharya S., Roy B., Chattopadhyay D.J., Mondal T.K., Nethaji M., Zangrando E., Das D.* // Inorg. Chem. – 2010. – **49**, N 7. – P. 3121 – 3129.
22. *Proft F.D., Geerlings P.* // Chem. Rev. – 2001. – **101**. – P. 1451 – 1464.
23. *Beyramabadi S.A., Eshtiagh-Hosseini H., Housaindokht M.R., Morsali A.* // Organometallics. – 2008. – **27**, N 1. – P. 72 – 79.
24. *Delchev V.B., Delcheva G.T.* // J. Struct. Chem. – 2007. – **48**, N 4. – P. 615 – 622.
25. *Eshtiagh-Hosseini H., Beyramabadi S.A., Housaindokht M.R., Morsali A.* // J. Mol. Struct.: THEOCHEM. – 2010. – **941**, N 1-3. – P. 138 – 143.
26. *Sıdır İ., Sıdır Y.G., Taşal E., Öğretir C.* // J. Mol. Struct. – 2010. – **980**, N 1-3. – P. 230 – 244.
27. *Dega-Szafran Z., Katrusiak A., Szafran M.* // J. Mol. Struct. – 2008. – **880**, N 1-3. – P. 69 – 76.
28. *Nuzhdin K.B., Nesterov S.V., Tyurin D.A., Feldman V.I., Wei L., Lund A.* // J. Phys. Chem. A. – 2005. – **109**, N 28. – P. 6166 – 6173.
29. *Brouwer A.M.* // J. Phys. Chem. A. – 1997. – **101**, N 19. – P. 3626 – 3633.
30. *Beyramabadi S.A., Morsali A., Javan Khoshkholgh M., Esmaeili A.A.* // J. Struct. Chem. – 2012 (accepted for publication).
31. *Frisch M.J. et al.* Gaussian 03, Revision B.03. – Gaussian, Inc.: Pittsburgh PA, 2003.
32. *Lee C., Yang W., Parr R.G.* // Phys. Rev. B. – 1988. – **37**, N 2. – P. 785 – 789.
33. *Tomasi J., Cammi R.* // J. Comput. Chem. – 1995. – **16**, N 12. – P. 1449 – 1458.
34. *Young D.C.* Computational Chemistry: A Practical Guide for Applying Techniques to Real – World Problems, John Wiley & Sons, Inc., 2001.
35. *Nielsen K.T., Harris P., Bechgaard K., Krebs F.C.* // Acta Crystallogr. – 2007. – **B63**. – P. 151 – 156.
36. *Shaheen F., Badshah A., Anjum S., Saqib A.* // Acta Crystallogr. – 2006. – **E62**. – P. m329 – m330.
37. *Fan L.-Q., Wu J.-H., Huang Y.-F., Ng S.W.* // Acta Crystallogr. – 2009. – **E65**. – P. m1209.
38. *Hou L.-F., Zhong Y., Mei Y., Fan J.* // Acta Crystallogr. – 2009. – **E65**. – P. m1694.
39. *Kropidlowska A., Ianszak J., Galaszewska J., Becker B.* // Acta Crystallogr. – 2007. – **E63**. – P. m1947.
40. *Santos Jr S., Guilardi S., Resende J.A.L.C., Rubinger M.M.M., Oliveira M.R.L., Ellena J.* // Acta Crystallogr. – 2003. – **E59**. – P. m77 – m79.
41. *Selvaraju R., Panchanatheswaran K., Thiruvalluar A., Parthasarathi V.* // Acta Crystallogr. – 1995. – **C51**. – P. 606 – 608.
42. *Jian F.-F., Wang Z.-X., Fun H.-K., Bai Z.-P., You X.-Z., Razak I.A., Chinnakali K.* // Acta Crystallogr. – 1998. – **C54**. – P. IUC9800044.
43. *Snehalatha M., Ravikumar C., Hubert Joe I., Sekar N., Jayakumar V.S.* // Spectrochim. Acta A. – 2009. – **72**, N 3. – P. 654 – 662.
44. *Salavati-Niasari M., Mirsattari S.N., Monajjemi M., Hamadanian M.* // J. Struct. Chem. – 2010. – **51**, N 3. – P. 437 – 443.